Water Research X 25 (2024) 100267

Contents lists available at ScienceDirect

Water Research X

journal homepage: www.sciencedirect.com/journal/water-research-x

Near-Complete Phosphorus Recovery from Challenging Water Matrices Using Multiuse Ceramsite Made from Water Treatment Residual (WTR)

Jianfei Chen [a], Jinkai Xue [a,*], Jinyong Liu [b], Seyed Hesam-Aldin Samaei [a], Leslie J. Robbins [c]

[a] Cold-Region Water Resource Recovery Laboratory (CRWRRL), Environmental Systems Engineering, Faculty of Engineering & Applied Science, University of Regina, Regina, SK S4S 0A2, Canada
[b] Department of Chemical & Environmental Engineering, University of California, Riverside, California 92521, United States
[c] Department of Geology, University of Regina, Regina, SK S4S 0A2, Canada

ARTICLE INFO

Keywords:
Eutrophication
circular economy
sludge valorization
waste valorization
water treatment
adsorbent
Sips isotherm
nutrient recovery

ABSTRACT

Water treatment residual (WTR) is a burden for many water treatment plants due to the large volumes and associated management costs. In this study, we transform aluminum-salt WTR (Al-WTR) into ceramsite (ASC) to recover phosphate from challenging waters. ASC showed remarkably higher specific surface area (SSA, 70.53 m^2/g) and phosphate adsorption capacity (calculated 47.2 mg P/g) compared to previously reported ceramsite materials (< 40 m^2/g SSA and < 20 mg P/g). ASC recovered over 94.9% of phosphate across a wide pH range (3 – 11) and generally sustained > 90% of its phosphate recovery at high concentrations of competing anions (i.e., Cl^-, F^-, SO_4^{2-}, or HCO_3) or humic acid (HA). We challenged the material with real municipal wastewater at 10°C and achieved simultaneous phosphate (>97.1%) and COD removal (71.2%). Once saturated with phosphate, ASC can be repurposed for landscaping or soil amendment. The economic analysis indicates that ASC can be a competitive alternative to natural clay-based ceramsite, biochar, or other useful materials. Therefore, ASC is an eco-friendly, cost-effective adsorbent for phosphate recovery from complex waters, shedding light upon a circular economy in the water sector.

1. Introduction

The large quantities of water treatment residual (WTR) produced during the coagulation process at drinking water treatment plants (DWTPs) are challenging to the utilities and local environment. Because aluminum salts are widely used as coagulants, sustainable management of aluminum salt-based WTR (Al-WTR) is particularly interesting to the industry. Traditionally, Al-WTR has been disposed of in local landfills, creating both financial and environmental burdens. Transforming this waste into ceramsite can be promising.

Ceramsite is traditionally made from clay or shale and can be used as lightweight aggregate, landscaping mulch, etc. (Liu et al., 2020). Al-WTR contains both skeleton materials (i.e., Al_2O_3 and SiO_2) and flux materials (e.g., Na_2O, CaO, Fe_2O_3, and K_2O) critical for ceramsite production. In addition, Al-WTR contains a higher content of organic matter (pore-forming) (Huang et al., 2023), making it an even better raw material for ceramsite than clay. Therefore, transforming Al-WTR into ceramsite can help the water sector reduce operating costs and environmental footprint, generate more revenue, and assist the ceramsite industry in addressing environmental and land use concerns, supporting a circular economy can be achieved. To date, few studies have used Al-WTR for ceramsite fabrication. Al-WTR-based ceramsite (**ASC**) can find many beneficial uses as an adsorbent, construction material, and landscaping mulch (Chen et al., 2024; Dong et al., 2021; Nguyen et al., 2022; Wang et al., 2019). In particular, given its abundant di-/tri-valent metal content (e.g., Al), ASC can be a promising adsorbent for phosphate and holds great potential for recovering the precious phosphorus (P) resource from eutrophic water and wastewater (Cheng et al., 2018; Wang et al., 2021). Due to the non-renewable nature of geological P deposits, a global P shortfall for industrial and agricultural needs is predicted by 2035 (Liu et al., 2021c; Pap et al., 2020). ASC offers an opportunity to obliterate the unbalanced distribution of P and facilitate sustainable development.

Herein, we systematically investigated the fabrication of ASC with a specific surface area (SSA) and phosphate adsorption capacity much higher than all previously reported ceramsite materials made from WTR. Experimental and theoretical analyses indicate that this material can be a cost-effective solution to tackle the phosphate challenge in eutrophic

* Correspondent author.
E-mail address: jinkai.xue@uregina.ca (J. Xue).

https://doi.org/10.1016/j.wroa.2024.100267
Received 23 August 2024; Received in revised form 16 October 2024; Accepted 17 October 2024
Available online 21 October 2024

waterbodies such as agricultural ponds. Economic analyses suggest that ASC may be a more affordable alternative to several commercial products such as clay ceramsite, tire crumb, and lightweight aggregate. This study would bring insights for transforming WTR into ceramsite can help water treatment plants: 1) reduce operating costs and environmental impact, 2) create new revenue opportunities, and 3) contribute to achieving a circular economy.

2. Results and discussion

2.1. ASC is an exceptional adsorbent for phosphate

ASC demonstrated exceptional performance compared to previously reported ceramsite materials. Its SSA and total pore volume were 70.53 m^2/g and 0.23 cm^3/g, respectively (Fig. 1A and Fig. S2A&B). Its pore size distribution ranged from 2 and 50 nm (Fig. 1A), with a peak at 7.7 nm (Fig. S2B). In contrast, Wang et al.'s ceramsite made from WTR and bentonite (7:3 wt%) had an SSA of 45.4 m^2/g (Wang et al., 2022), and the modified commercial ceramsite in Wu et al. (2020a) had a pore size of 7.7 to 14.8 nm and a pore volume of 0.067 – 0.151 cm^3/g. Benchmarking against previously reported ceramsite materials (made from red mud, slag, clay, etc.(Cheng et al., 2018; Li et al., 2023; Lin et al., 2021; Liu et al., 2021a; Liu et al., 2021b; Wu et al., 2020a). with a large SSA and high phosphate adsorption capacity, we found ASC in this study had the largest SSA (Fig. 1B&C and Table S7). A large SSA increases the number of adsorption sites. To further explore the adsorption behaviors, experimental data were fitted to the kinetic and isotherm models as described in SI Texts S3 and S6. Isotherm experiments (Fig. S4D) proved an experimentally determined maximum phosphate adsorption capacity of 42.9 mg PO_4^{3-}/g (or 14.3 mg P/g) of ASC, and the Sips model predicted a maximum absorption capacity at 10°C to be 141.7 mg PO_4^{3-}/g (or 47.23 mg P/g), making this WTR-derived ceramsite the best performer in both Fig. 1B&C. Adsorption experiments for kinetic analysis were conducted using three initial phosphate concentrations (i.e., 5, 30, and 50 mg PO_4^{3-}/L) (Fig. S4A). These concentrations are significantly higher than typical environmental P levels. In Canada, water bodies with a total phosphorus (TP) concentration of 0.035 – 0.100 mg P/L (equivalent to 0.107 – 0.306 mg PO_4^{3-}/L) are categorized as eutrophic, and waters with [TP] > 0.100 mg P/L (or > 0.306 mg PO_4^{3-}/L) is hyper-eutrophic (Water Science and Technology Directorate, 2011). At 10°C, after approximately 11 hrs, adsorption stabilized at 0.74, 4.22, and 8.13 mg PO_4^{3-}/g, corresponding to a phosphate recovery rate of 97.6, 93.9, and 91.9%, respectively (Fig. S4A). Adsorption kinetics and XPS analyses suggest that the phosphate adsorption onto ASC was primarily driven by strong chemical adsorption between surface active sites (e.g., Al^{3+}, Ca^{2+}) and functional groups (SI Text S6) (Lin et al., 2021; Ma et al., 2022). Multiple mechanisms can be involved, including ligand exchange, chemical deposition, and inner-sphere complexation. FTIR analysis confirmed the presence of phosphate on the adsorbent surface, while XPS analysis further supported these findings by demonstrating changes in binding energies and chemical interactions between phosphate and surface groups such as Ca, Al, and oxygenated functional groups. Detailed discussion on the adsorption mechanisms can be found in Texts S6 to S8.

On the other hand, the surface of ASC was among the least active, as indicated by the ratio of phosphate adsorption capacity (either experimentally determined or model-predicted) and SSA in Fig. 1D. We anticipate that our ASC's performance can be further enhanced by increasing the density of active sites on the surface. XRD analysis (Fig. S2D) showed that the main crystalline phases of ASC were quartz (SiO_2), muscovite ($KAl_2Si_3AlO_{10}(OH)_2$), albite ($NaAlSi_3O_8$), sanidine ($KAlSi_3AlO_8$), and a small amount of calcite ($CaCO_3$), which help explain the good phosphate adsorption by ASC and suggest possible

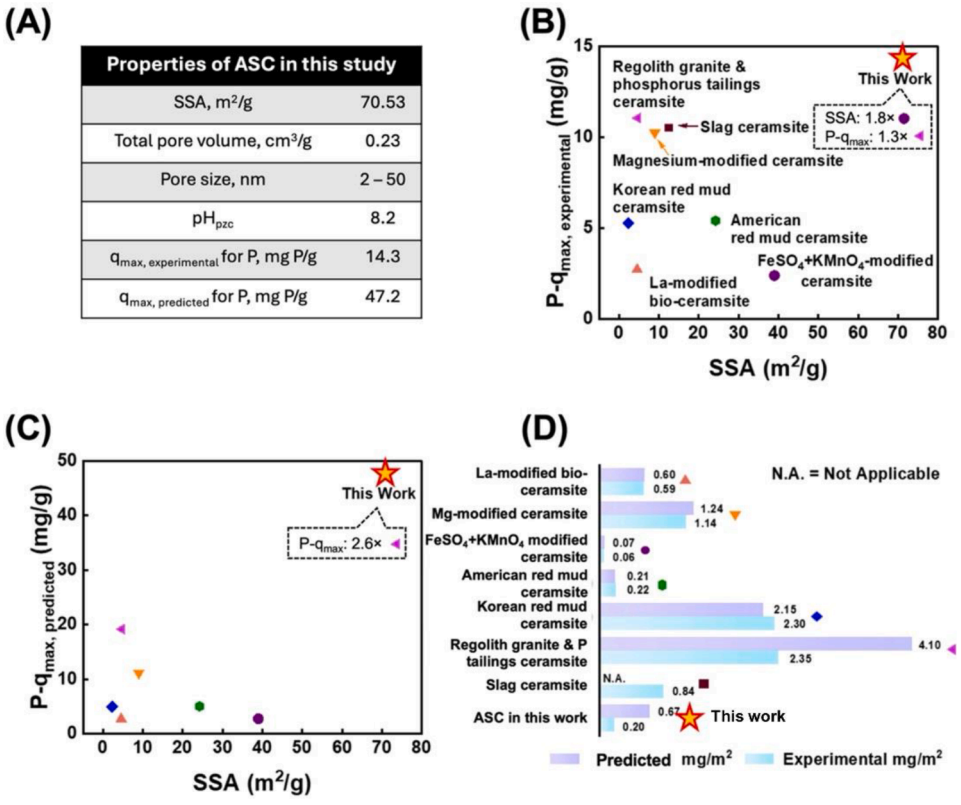

Fig. 1. Properties of ASC (A) and benchmarking its SSA and phosphate adsorption against ceramsite materials in the literature: experimentally determined maximum phosphate adsorption capacity and SSA (B), model predicted maximum phosphate adsorption capacity and SSA (C), and the ratio of phosphate adsorption capacity to SSA (D). The literature data are mean values or figure read-offs collected from published articles. P-q_{max} represents the maximum adsorption capacity in the unit of mg P/g ceramsite.

opportunities for improvement. A few strategies can be explored include: 1) adjusting the fabrication conditions, 2) adding certain auxiliary materials (e.g., eggshell) to the recipe, or 3) modifying the surface after sintering by incorporating lanthanum, iron, or other hard acid metals.(Cheng et al., 2018; Wang et al., 2023a; Wang et al., 2018; Wu et al., 2019; Wu et al., 2020b)

Regardless of future improvements, the high phosphate adsorption capacity achieved in this study inspires us to envision ASC's potential application for remediating eutrophic waterbodies, such as agricultural ponds for livestock (dugouts) and stormwater ponds. For a small dugout with a volume of one million Imperial gallons (4.5 million litres), which is typical in Western Canada (Agriculture and Agri-Food Canada, 2020; Alberta Agriculture and Forestry, 2015), if the phosphate concentration is 0.1 mg P/L (highly eutrophic (Water Science and Technology Directorate, 2011)), merely 10 kg of ASC will be needed to recover the phosphorus from the polluted water. For an extremely large dugout of 30 million litres of water (Agriculture and Agri-Food Canada, 2020), 63 kg of ASC would suffice. Each tonne of ASC will recover 141.6 kg of phosphate. If we take a more conservative approach, using the phosphate adsorption capacity of 14.3 mg P/g achieved in our experiments, the 4.5-million-litre and 30-million-litre dugouts will require 32 and 210 kg of ASC, respectively. However, real waters are complex – will this material robustly recover phosphate under the influence of various factors?

2.2. What will impact phosphate adsorption onto ASC?

We examined several factors that may influence phosphate adsorption onto ASC, including ASC dosage, pH, temperature, co-existing anions and NOM, and regeneration cycles.

Effect of ASC dosage: The effect of adsorbent dosage on phosphate adsorption was evaluated (Fig. 2A). As the adsorbent dosage increased from 2 to 10 g/L, the removal significantly increased from ~78 to 100%, obviously owing to the increased total surface area and number of adsorption sites. However, the equilibrium adsorption capacity decreased from 3.68 to 0.91 mg PO_4^{3-}/g as the dosage increased, suggesting an abundance of unoccupied sites. Phosphate removal exceeded 95% at an ASC dosage of 6 g/L, with a further increase in adsorbent dosage providing only marginal improvement. Hence, an ASC dosage of 6 g/L was selected for subsequent experiments.

Effect of pH: pH affects the speciation of the adsorbate in this study (Fig. S6), which, in turn, affects the adsorption efficiency. We studied the adsorption of (total) phosphate (the sum of H_3PO_4, $H_2PO_4^-$, HPO_4^{2-}, and PO_4^{3-}) by ASC over a wide pH range (3.0 – 11.0) (Fig. 2B). In this pH range, $H_2PO_4^-$ and HPO_4^{2-} are the dominant species (Fig. S6) (Kumar et al., 2019). pH influences the surface charge of the adsorbent, which further influences phosphate adsorption. The pH_{pzc} of ASC was close to 8.2 (Fig. S2C), indicating that the adsorbent surface was positively charged at pH < 8.2. Fig. 2B indicates stable and excellent phosphate adsorption (94.9 – 97.0%) across all tested pH levels at low phosphate levels (10 mg PO_4^{3-}/L). It follows that at pH < pH_{pzc}, the ceramsite surface underwent protonation, allowing for electrostatic attraction between the positively charged ceramsite surface and PO_4^{3-}. Nonetheless, the high phosphate adsorption (94.9%) by ASC at pH = 11.0 was due to the stronger affinity between phosphate ions and di-/tri-valent metals on ASC surface. Compared with OH^- ions, PO_4^{3-} ions have a higher charge density and smaller ionic radius. The same reason allowed phosphate ions to replace the alkaline species (e.g., OH^-) that had been initially bound to the di-/trivalent metals on the pristine ceramsite surfaces (Qiu et al., 2019). The ligand exchange phenomenon resulted in a substantial pH increase in all systems after phosphate adsorption (Fig. 2B). Other mechanisms might also contribute to phosphate adsorption onto ASC, such as calcite (the XRD result in Fig. S2D), which can adsorb phosphate. In conclusion, ASC demonstrated near-complete phosphate adsorption across a broad pH range at low temperatures, and the effect of pH was negligible.

Effect of temperature: Adsorption experiments were performed with three initial phosphate concentrations (10, 50, and 100 mg PO_4^{3-}/L) at

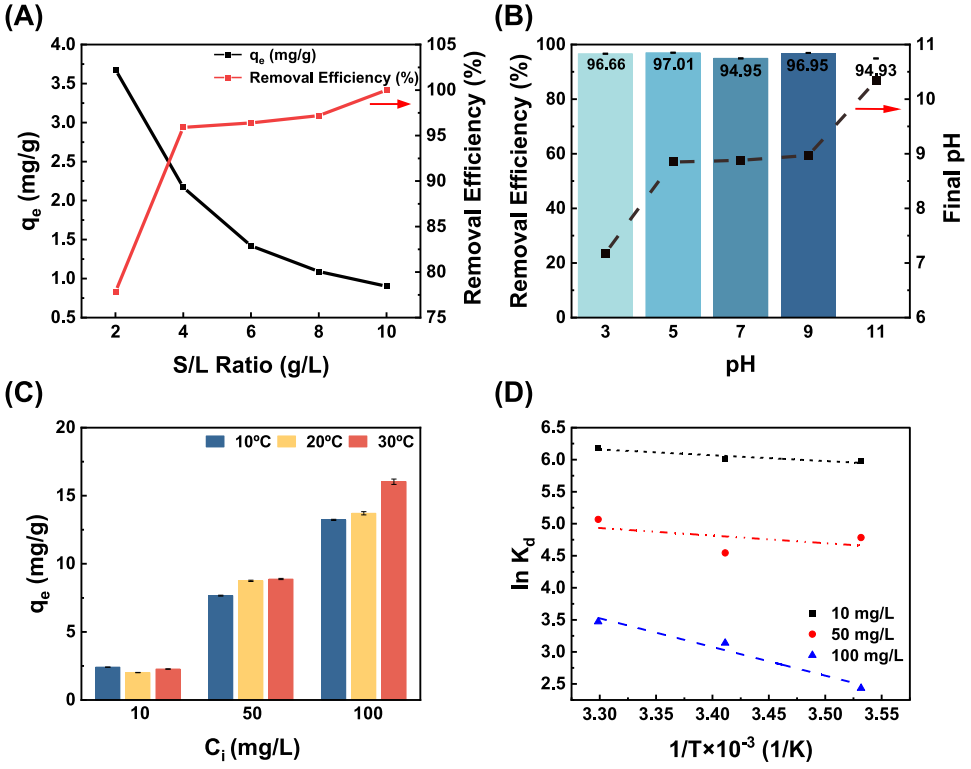

Fig. 2. Effects of ASC dosage (A), pH (B), temperature on phosphate adsorption onto ASC (C), and van't Hoff plot for phosphate adsorption onto ASC with different initial phosphate concentrations (D). Data are presented as mean values of sample duplicates ± standard deviation (each sample replicate was measured three times to get a mean first). q_e is the phosphate adsorption capacity at adsorption equilibrium (mg/g).

three temperatures (10, 20, and 30°C) (Fig. 2C). For 10 mg PO_4^{3-}/L, the effect of temperature was negligible, while the higher temperature appeared to slightly benefit phosphate adsorption at initial concentrations of 50 and 100 mg PO_4^{3-}/L. The van't Hoff equation was used to compute Gibbs free energy change (ΔG), enthalpy change (ΔH), and entropy change (ΔS) for phosphate adsorption (Fig. 2D and Table S6). As indicated by the negative values of ΔG, the adsorption process is spontaneous and favoured at higher temperatures. The positive ΔS values suggest a strong affinity between ASC and phosphate, as well as an increase in randomness index at the solid/liquid interface during adsorption at a higher temperature (Zeng et al., 2023).

Effect of co-existing anions: Anions in water can influence phosphate adsorption due to their competition for active sites (Fig. 3A). However, the co-existing anions in our experiments only slightly impacted phosphate recovery, with the order of $Cl^- < SO_4^{2-} < F^- < HCO_3^-$. ASC generally maintained >90% phosphate recovery in the presence of competing anions, with only two exceptions (at 30 mM F^- or HCO_3^-). In the presence of 15 mM Cl^- or SO_4^{2-}, ASC achieved 96.7 and 95.3% phosphate removal, respectively. When the concentrations of these anions were doubled (30 mM), the inhibition of phosphate adsorption increased slightly (e.g., from 4.7 to 5.7% by SO_4^{2-}). This confirmed the formation of inner-sphere mono-dentate or bi-dentate complexes during phosphate adsorption (Zhang et al., 2017). Among all the tested anions, HCO_3^- exhibited the most significant impact on phosphate adsorption, reducing it from 96.5% (at 0 mM HCO^{3-}) to 90.4% (at 15 mM HCO^{3-}) and further to 85.2% (at 30 mM HCO^{3-}). The results were similar to those of a previous study using katoite adsorbent (Cheng et al., 2022). Due to the similarity of HCO_3^- and $H_2PO_4^-$, the anions are readily adsorbed via inner/outer-sphere complexation, which is crucial for understanding their competitive interaction on adsorbent surfaces (Koh et al., 2020). Moreover, F^- caused a notable decrease in phosphate removal (e.g., from 97.4% at 0 mM to 86.5% at 30 mM F^-), likely due to its strong affinity towards metal-active sites (Wan et al., 2021). Metallic-modified (e.g., La^{3+}, Al^{3+}, and Fe^{3+}) adsorbents are commonly inhibited by background pollutants in water despite their Lewis acid-base interaction-induced high selectivity for phosphate (Wang et al., 2023b; Zhu et al., 2024). Such inhibition was also observed when natural zeolite or clay modified with calcium hydroxide was used as an adsorbent (Ma et al., 2012; Mitrogiannis et al., 2017). The slight inhibition of phosphate adsorption observed in our experiments is, therefore, not unexpected and should not pose a significant deterrent for the application of ASC. Overall, ASC showed excellent phosphate selectivity, maintaining over 85% (generally over 90%) of its adsorption capacity at high concentrations of competing anions. This suggests phosphate adsorption on ASC was primarily driven by chemisorption (as previously assumed) rather than outer-sphere complexation via electrostatic attraction. The impact of water hardness (i.e., Mg^{2+} and Ca^{2+}) was not investigated in the present study, which commonly promotes phosphate adsorption according to the literature (Li et al., 2023; Lin et al., 2017).

Effect of co-existing natural organic matter (NOM): NOM may also influence phosphate adsorption in natural water systems. Contrary to expectations (Wang et al., 2023a), our experiments showed a negligible impact of HA (representing NOM) on phosphate adsorption (Fig. 3A), similar to recent studies using magnesium-stirred biochar and lanthanum-modified bio-ceramsite (Liu et al., 2021b; Luo et al., 2022). In contrast, Liu et al. (2021b) observed significantly inhibited phosphate adsorption by 50 and 100 mg/L of HA. Such high concentrations of HA, however, are less environmentally relevant. Comparative experiments indicated that phosphate interfered with HA adsorption onto ACS (Fig. 3B and Fig. S1B). Such interference was the most significant when the HA concentration was low (1 mg/L) and became almost negligible when the latter increased to 20 mg/L. This pseudo-unilateral impact of phosphate on HA competing for adsorption sites on ceramsite suggests that the HA adsorbed on ceramsite may offer additional adsorption sites for phosphate, possibly through electrostatic attraction between amine groups of HA and phosphate ions. Considering the release of di- or tri-valent cations from the ceramsite, bridging and complexation could also play a role in facilitating phosphate adsorption onto HA-loaded ceramsite. Further experimental and modelling studies could help unveil the interaction between HA and phosphate on the ceramsite surface

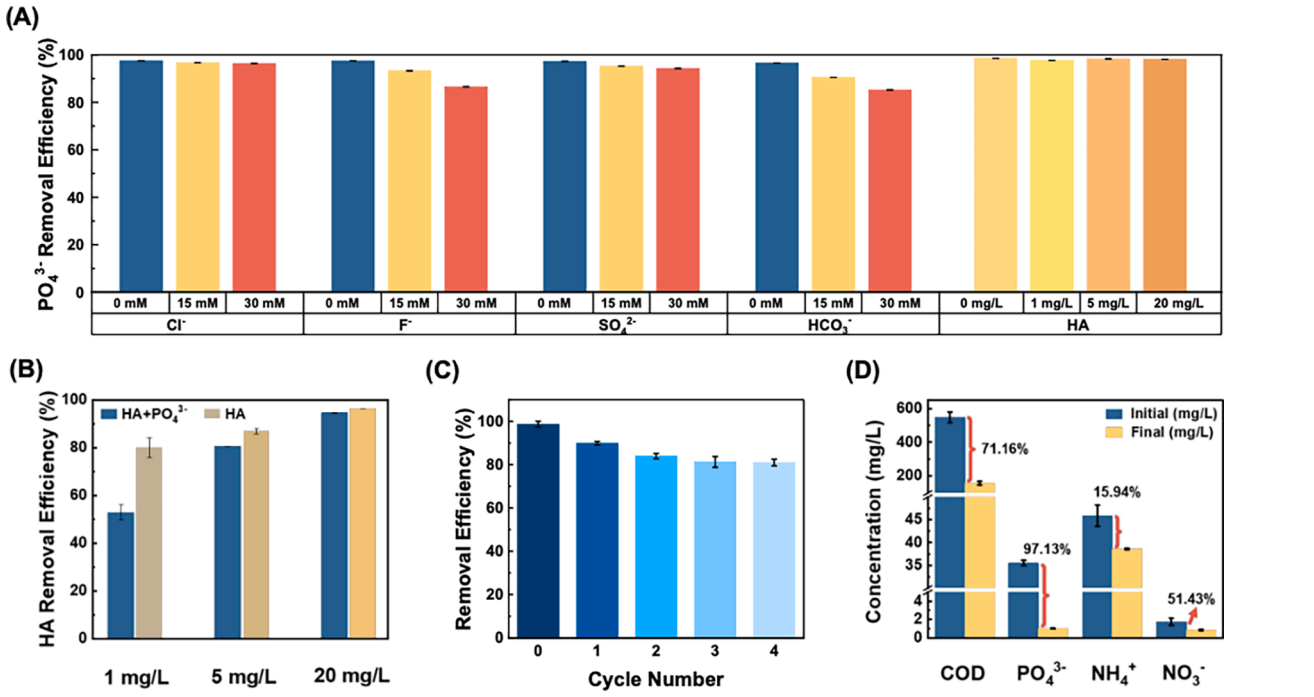

Fig. 3. Effects of co-existing anions and NOM on phosphate adsorption by ASC (A); the HA removal (%) by ASC with and without phosphate (10 mg PO_4^{3-}/L, 10°C, 6 g ASC/L, pH=7.5, @150 rpm for 72 hrs)(B); regeneration of ASC using 1.0 M NaOH (C); and ASC for real municipal wastewater treatment (6 g ASC/L, pH = 7.5, at 10°C, @150 rpm for 72 hrs) (D). Data are presented as mean values of sample duplicates ± standard deviation (each sample replicate was measured three times to get a mean first).

in greater detail. Regardless, ASC has demonstrated its potential for phosphate recovery from complex water matrices under cold conditions.

Effect of regeneration: Two solutions (1.0 M NaOH or HCl) and RO water were tested to desorb phosphate from spent ASC. After 12 hrs of desorption, 94.2 ± 1.4% of the adsorbed phosphate was removed from ASC using 1.0 M NaOH, which was more effective than what 1.0 M HCl achieved. Therefore, NaOH was chosen as the regeneration agent (Li et al., 2022). After four reuse cycles, phosphate removal declined from 98.7 (pristine) to 80.6% (Fig. 3D). This decline can be attributed to multiple reasons, such as leaching loss of active elements such as Al and Ca under strongly alkaline conditions, depletion of active sites due to chemical precipitation between phosphate ions and di- or tri-valent metals on the ASC surface, or phosphate ions trapped in deep pores (which makes it hard to wash adsorbed phosphate out during desorption). The phosphate-rich eluent can be used to produce fertilizers such as struvite (Li et al., 2021). Further investigation is warranted to minimize the use of strong eluent and reduce contact times in regenerating spent ASC. Although ASC exhibited good reusability, it may not need regeneration at all. Instead, spent ceramsite can be repurposed, such as being used as a nutrient-rich landscaping mulch, an inexpensive alternative to wood chips or toxic tire shreds (Ziajahromi et al., 2023), offering additional environmental and economic benefits (more discussion in the following sections). Furthermore, P-solubilizers, such as phosphate-solubilizing bacteria, have been proven to efficiently release phosphorus from various forms, including Al-bound phosphate, and Al-P fertilizers have outperformed Ca-P fertilizers in long-term field experiments (Aliyat et al., 2022; Shi et al., 2024).

2.3. Phosphate recovery from municipal wastewater under cold conditions?

ASC was used to recover phosphate from real municipal wastewater (Fig. 3D). After removing suspended solids, the wastewater's pH (7.5) and initial phosphate concentration (35.5 mg PO_4^{3-}/L) were measured. Over 97.1% of phosphate and 71.2% of COD from the real wastewater were simultaneously removed by 6 g/L ASC at 10°C, resulting in a final phosphate concentration of 0.34 mg P/L (Fig. 3B and Table S8). Hence, ASC shows promise for recovering phosphate from actual wastewater under cold conditions or for polishing treated wastewater (Fig. 4). To meet stringent discharge limits (0.05 – 0.3 mg P/L) (Shan et al., 2020), slightly increasing the adsorbent dosage or raising the operating temperature should help. This requires validation by running real water in a pilot-scale system to determine the optimal operating conditions.

Therefore, ASC can be an extraordinary adsorbent for recovering phosphate from various water matrices, such as municipal wastewater, lagoons, and dugouts (Fig. 4). It offers municipalities, agricultural producers, and industries with an inexpensive and facile approach to address phosphate pollution. Additionally, spent ASC can become a valuable product for beneficial uses. ASC enriched with phosphate can be used for landscaping or soil amendment, relocating phosphate from polluted waters to where it is needed (Fig. 4). Moreover, ASC can also find applications in stormwater management as a bioretention cell medium or storage medium or in the construction industry as a lightweight aggregate. The question is – Is this material economically affordable?

2.4. Economic analysis of ASC

A preliminary (oversimplified) cost analysis is conducted herein based on the framework described previously (He and Wang, 2019). Each tonne of ASC required 15.9 tonnes of raw WTR (10wt% solids) and 0.4 tonnes of clay. The direct production cost per tonne of ASC is broken down in Table S9. However, due to the inconsistencies in lab-scale equipment and variations in the fabrication process, the power cost of each tonne of ASC was estimated using the instruments available in our lab-scale setup. The primary cost results from the dewatering and drying process, which accounts for 82.8% of the total cost. This cost can be further reduced by employing appropriate freeze-thaw and air-drying methods. It is assumed that other costs associated with ASC production, such as labor and equipment, are comparable to the total direct production cost (Nematian et al., 2021), making the overall production cost for ASC CA$171.5 × 2 = CA$343 per tonne. Considering the service fee paid by DWTPs for sludge disposal and potential subsidies or incentives from federal and provincial governments, the actual cost of ASC may be lower. Given ASC's potential as a material for water filtration and landscaping mulch, we collected the prices of the common materials for these purposes on the Canadian market by web searching, emailing, or calling the vendors (Fig. 5). ASC holds advantages over many of these materials, including biochar, commercial ceramsite made from clay, and tire crumb. Notably, natural clay-based lightweight aggregate (essentially ceramsite) is priced at ~CA$600 per tonne. ASC could offer good profitability if priced below CA$600. Moreover, if intended as landscaping mulch or soil amendment, each tonne of ASC can recover up to 141.6 kg of phosphate from eutrophic waters prior to final use, providing further environmental and economic benefits.

3. Conclusion and Implications

Al-WTR-based ceramsite (ASC) is a promising adsorbent for

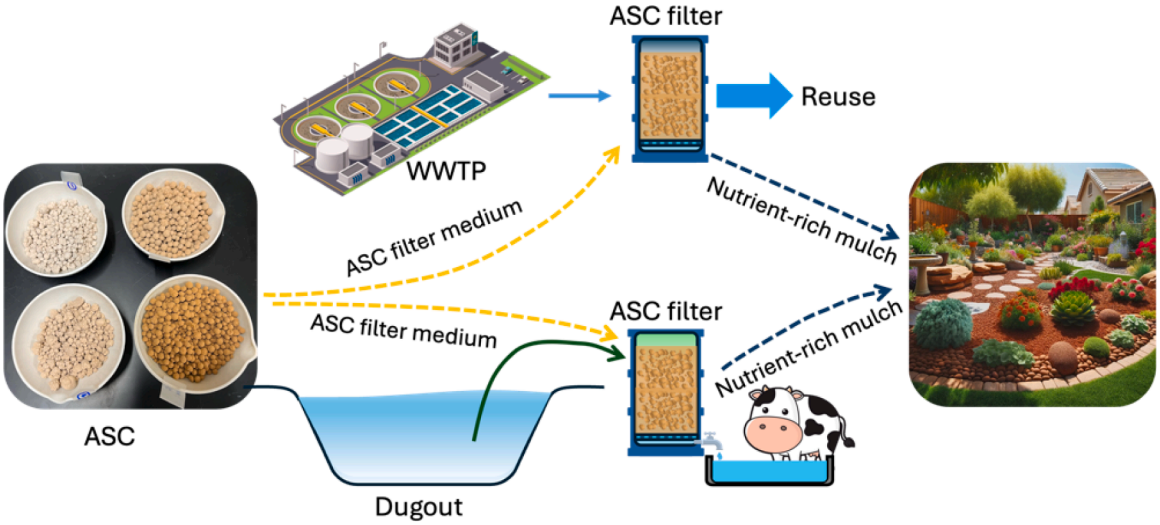

Fig. 4. Illustration of ASC's versatility.

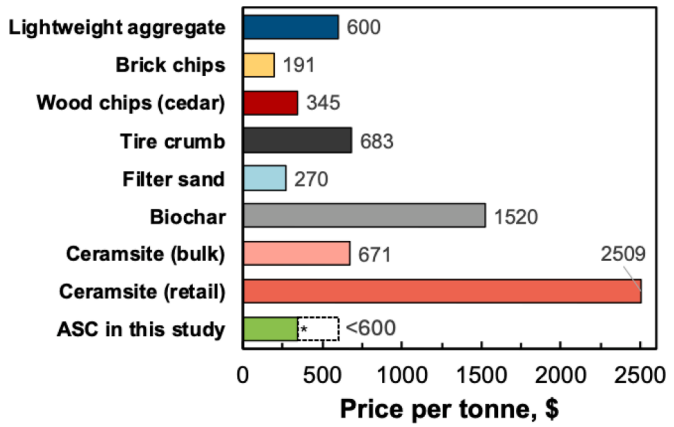

Fig. 5. Prices of materials that may be replaced with ASC on the Canadian market as of April 2024 (*estimated break-even price, CA$343).

phosphate recovery and eutrophication control. ASC exhibited a substantially higher specific surface area (SSA) and phosphate adsorption capacity than all previously reported ceramsite materials, which emphasizes the importance of finetuning all fabrication factors. It demonstrated broad pH adaptability and strong phosphate selectivity in complex water matrices, even at low temperatures, such as testing in real municipal wastewater at a low temperature (10°C). The adsorption experiments and Sips isotherm model suggested a theoretical maximal phosphate adsorption capacity of 141.7 mg PO_4^{3-}/g under cold conditions. The excellent phosphate adsorption of ASC in complex waters under cold conditions has solid implications for phosphorus recovery or pollutant removal from engineered (e.g., WWTPs, stormwater ponds, and dugouts) and natural water systems (e.g., lakes). The dominant adsorption mechanisms for phosphate onto ASC are chemical deposition, inner-sphere complexation, and ligand exchange. This waste-derived product is particularly appealing because it does not require regeneration once saturated with non-hazardous pollutants such as phosphate and NOM. Instead, the spent ceramsite can be repurposed for other beneficial applications, such as lightweight concrete aggregate and safe, fertilizing landscaping mulch to replace tire shreds (toxic) or wood chips. Multiple sectors could benefit from this material. For instance, WWTPs may use it to remove nutrients, microplastics, and emerging pollutants. Other wastes rich in silica (e.g., glass) can be used to replace the clay used in this study, further improving the environmental and social benefits. More research is needed to explore such possibilities and improve the material's performance. This study showcases the practicality of repurposing Al-WTR for beneficial uses. It sheds light on building a circular economy in the water sector and promoting industry sustainability.

4. Methods

4.1. Materials

The Al-WTR was collected from the Buffalo Pound Water Treatment Plant (BPWTP), which uses PACl as the primary coagulant. The wastewater (primary influent) was collected from the local wastewater treatment plant (WWTP). All chemicals were purchased from either Fisher Scientific or VWR. Details are shown in Supporting Information (SI) Text S1.

4.2. Fabrication of ceramsite

The raw material (RM) was Al-WTR, and the auxiliary material (AM) was bentonite clay (clay). Approximately 90.8 ± 1.1wt% of the raw Al-WTR was water, while the solid content had a higher volatile fraction (61.9wt% organics) than the fixed (38.1wt% inorganics). The clay ensured sufficient formation of the liquid phase and easy mouldability (Hu et al., 2023). The main mineral compositions of the raw materials are as follows (Table S10): Al-WTR (42.3% Al_2O_3, 14.8% SiO_2, 0.5% K_2O, 0.6% MgO, 2.3% CaO, 1.4% Fe_2O_3, 0.2% Na_2O, 0.6% P_2O_5) and clay (13.7% Al_2O_3, 55.8% SiO_2, 5.9% K_2O, 1.6% MgO, 2.4% CaO, 3.8% Fe_2O_3, 1.8% Na_2O, 0.2% P_2O_5). Al-WTR and clay were dried at 105°C for 72 hrs and then ground to pass through Mesh #100 sieves (pore size equivalent to 0.15 mm). The completely mixed raw meal was gradually poured into a granulator to prepare raw granules with particle sizes of < 3 mm. RO water was sprayed during the granulation process. Raw meals made with a range of Al-WTR: clay mass ratios were used. The obtained granules were then pre-dried at 105°C for 12 hrs before they were transferred into a muffle furnace for sintering (Fig. 6).

To efficiently improve the fabrication process, Taguchi Experimental Design method was used. The fabricating factors were Al-WTR: clay mass ratio (wt%, C_1), preheating time (min, C_2), preheating temperature (°C, C_3), sintering time (min, C_4), sintering temperature (°C, C_5, between 800 and 1200°C), and heating rate (°C/min, C_6). Each factor was examined at three levels, creating an L27 (6^3) orthogonal design. The Brunauer-Emmett-Teller specific surface area (BET-SSA) of the ceramsite was used as the evaluation index given by its direct impact on adsorption. Minitab 20 software was used for data analyses. Details in SI Text S4. Through the Taguchi Experiments, the ceramsite with batch ID ASC#25 had the largest SSA and could be the best adsorbent among all the tested batches. To assess the heavy metal leaching risk of ASC, leaching experiments were conducted at pH = 2.0 (Table S3). ASC met the limits specified by the US EPA (USEPA, 2004). Heavy metal analyses were done at Shiyanjia Lab, China.

4.3. Adsorption experiments

The ceramsite granules were first rinsed with RO water (3 – 5 times) to remove impurities, followed by 20-min shaking for further purification, then dried at 105°C for 24 hrs before being used for adsorption. Dried ceramsite was stored in a sealed desiccator. Adsorption experiments were conducted in an incubator shaker (HNY-2102C, Honour Instrument Co., Ltd., China) at 150 ± 1 rpm, and the pH of the synthetic solution was adjusted with 1.0 M HCl or NaOH solutions as appropriate. At every predetermined time point, the suspension was collected and filtered through a pre-rinsed syringe filter (0.45-μm mixed cellulose esters). The total phosphate (TP) concentration was measured by a pre-calibrated spectrophotometer (HACH DR 3900), using the PhosVer®3 kit. Phosphate concentrations of all suspension samples were measured in duplicates. The detailed measurement methods of chemical oxygen demand (COD), ammonia (NH_4^+), nitrate (NO_3^-), and HA are summarized in Text S2. The adsorption of phosphate and HA onto the container walls was experimentally determined to be negligible (Fig. S1).

Adsorption kinetics were studied with different initial phosphate concentrations (i.e., 5, 30, and 50 mg/L) at 10°C for 72 hrs (pH = 7.5 and S/L ratio = 6.0 g/L). Samples were taken at different times (0 – 72 hrs) for model fitting. For the adsorption isotherms, approximately 0.18 g of the adsorbent was added into 30 mL of phosphate solution (i.e., S/L ratio = 6 g/L) with initial phosphate concentrations ranging from 5 to 900 mg PO_4^{3-}/L in polypropylene bottles at 10°C and shaken at 150 rpm for 72 hrs. The pH of the solution was adjusted to 7.50 ± 0.02. Four adsorption kinetics (i.e., pseudo-first order, PFO; pseudo-second-order, PSO; Elovich; and intra-particle diffusion, IPD), three adsorption isotherms (i.e., Langmuir, Freundlich, and Sips), and adsorption thermodynamics were employed. Subsequent adsorption experiments were conducted with different pH values (3.0 – 11.0 with 2-unit increments), solid: liquid ratios (S/L ratio, 2.0 – 10.0, 2-unit increments), temperatures (10, 20, and 30°C), contact times (0 – 72 hrs), and initial concentrations of phosphate (10, 50, and 100 mg PO_4^{3-}/L). Additionally, the effects of coexisting anions (i.e., Cl^-, F^-, SO_4^{2-}, or HCO_3^-) and natural organic matter (NOM, i.e., humic acid, HA) on phosphate adsorption were examined. The concentrations were set at 0, 15, or 30 mM for

Fig. 6. The workflow of the ACS fabrication.

anions and 1, 5, or 20 mg/L for HA. The details are shown in Text S3. All samples were duplicated.

4.4. Adsorbent regeneration

A series of four-cycle adsorption-desorption experiments were conducted. ASC (0.18 g) was dosed into 30 mL of phosphate solution (10 mg PO_4^{3-}/L) for 48 hrs at pH = 7.5 and 10°C. For desorption, the exhausted adsorbent was regenerated using 30 mL of 1.0 M HCl or NaOH solution, followed by RO water rinsing. After regeneration, the adsorption and desorption processes were repeated under the same operating conditions.

4.5. Material characterization

The ceramsite was characterized for its morphology, surface charge, crystalline composition, and phosphate adsorption. Details on BET, pH_{PZC}, X-ray diffraction (XRD), Fourier-transform infrared spectroscopy (FTIR), XPS (Shiyanjia Lab, China), and scanning electron microscopy coupled with energy-dispersive X-ray spectrometry (SEM-EDS) are provided in SI Text S5. Unless otherwise indicated, all measurements/analyses in this study were done at the University of Regina.

CRediT authorship contribution statement

Jianfei Chen: Writing – original draft, Visualization, Validation, Methodology, Investigation, Formal analysis. **Jinkai Xue:** Writing – review & editing, Writing – original draft, Visualization, Validation, Supervision, Resources, Project administration, Methodology, Investigation, Funding acquisition, Formal analysis, Conceptualization. **Jinyong Liu:** Writing – review & editing. **Seyed Hesam-Aldin Samaei:** Writing – review & editing, Writing – original draft, Validation. **Leslie J. Robbins:** Writing – review & editing.

Declaration of competing interest

The authors declare that they have no known competing financial interests or personal relationships that could have appeared to influence the work reported in this paper.

Acknowledgements

This study was supported by the Natural Sciences and Engineering Research Council of Canada (NSERC) through the NSERC Discovery Grant, NSERC Alliance Grant, NSERC Alliance International Catalyst Grant, Mitacs Accelerate Grant, Canada Foundation for Innovation (CFI) - John R. Evans Leaders Fund (JELF), Prairies Economic Development Canada (PrairiesCan) Regional Innovation Ecosystems (RIE) program, Innovation Saskatchewan, and the University of Regina (UofR) Vice President Research Discretionary Funds. We thank Buffalo Pound Water Treatment Corporation (BPWTC) for their generous funding support and field support. We thank the City of Regina and EPCOR for providing us with wastewater samples for our experiments. We thank Mr. Ben Lichtenwald, the Lab Instructor in Environmental Systems Engineering, for his invaluable support during sample preparation. S. S. and J. C. would thank the Saskatchewan Innovation and Excellence Graduate Scholarship and the UofR Faculty of Graduate Studies and Research (FGSR) Graduate Teaching Assistantship Award. J. C. thanks the UofR FGSR Asia Pacific Studies Scholarship. A natural language artificial intelligence (AI) chatbot, ChatGPT (Version 4.0, OpenAI), has been used to polish the language of this paper. We also acknowledge the edits made by CRWRRL's students Ms. Parnian Mojahednia and Ms. Lin Zhang, PDF Dr. Bin Wang, and Mr. Blair Kardash from BPWTC.

Supplementary materials

Supplementary material associated with this article can be found, in the online version, at doi:10.1016/j.wroa.2024.100267.

Data availability

The data that support the findings of this study are available within the paper and its Supplementary Information. Source data for all graphs are provided in this paper.

References

Agriculture and Agri-Food Canada, 2020. Farm surface water management. Government of Canada.

Alberta Agriculture and Forestry, 2015. Quality Farm Dugouts. Alberta Government, Edmonton, pp. 17–30.

Aliyat, F.Z., Maldani, M., El Guilli, M., Nassiri, L. and Ibijbijen, J.J.M. 2022. Phosphate-solubilizing bacteria isolated from phosphate solid sludge and their ability to solubilize three inorganic phosphate forms: Calcium, iron, and aluminum phosphates. 10(5), 980.

Chen, J., Samaei, S.H.-A., Rahman, R., Robbins, L.J., Xue, J., 2024. Toward a Circular Economy in Water Treatment: Upcycling Aluminum Salt-Based Water Treatment Residual into An Effective Adsorbent–Ceramsite. ACS ES&T Water.

Cheng, G., Li, Q., Su, Z., Sheng, S., Fu, J., 2018. Preparation, optimization, and application of sustainable ceramsite substrate from coal fly ash/waterworks sludge/oyster shell for phosphorus immobilization in constructed wetlands. Journal of Cleaner Production 175, 572–581.

Cheng, P., Liu, Y., Yang, L., Wang, X., Chi, Y., Yuan, H., Wang, S., Ren, Y.-X., 2022. Adsorption and recovery of phosphate from aqueous solution by katoite: Performance and mechanism. Colloids and Surfaces A: Physicochemical and Engineering Aspects 655, 130285.

Dong, B., Liu, J., Hong, S., Zhang, Y., Wang, Y., Xing, F.J.C. and Materials, B. 2021. Core-Shell structured ceramsite made by excavated soil and expanded perlite through cold-bonded technology. 306, 124941.

He, B., Wang, G., 2019. Is ceramsite the last straw for sewage sludge disposal: a review of sewage sludge disposal by producing ceramsite in China. Water Science & Technology 80 (1), 1–10.

Hu, N., Lv, Y., Luo, B., Ye, Y., Fu, F., Jia, J., Ou, Z., Li, J., 2023. Preparation and performance of porous ceramsite for Ag+ removal in sewage treatment with total phosphorus tailings. Journal of Cleaner Production 413, 137515.

Huang, C., Yuan, N., He, X., Wang, C., 2023. Ceramsite made from drinking water treatment residue for water treatment: a critical review in association with typical ceramsite making. Journal of Environmental Management 328, 117000.

Koh, K.Y., Zhang, S., Chen, J.P., 2020. Hydrothermally synthesized lanthanum carbonate nanorod for adsorption of phosphorus: Material synthesis and optimization, and demonstration of excellent performance. Chemical Engineering Journal 380, 122153.

Kumar, P.S., Korving, L., van Loosdrecht, M.C., Witkamp, G.-J., 2019. Adsorption as a technology to achieve ultra-low concentrations of phosphate: Research gaps and economic analysis. Water Research X 4, 100029.

Li, J., Li, B., Yu, W., Huang, H., Han, J.-C., Huang, Y., Wu, X., Young, B., Wang, G., 2022. Lanthanum-based adsorbents for phosphate reutilization: Interference factors, adsorbent regeneration, and research gaps. Sustainable Horizons 1, 100011.

Li, W., Cai, G., Luo, K., Zhang, J., Li, H., Li, G., Zhang, J., Chen, X., Xie, F., 2023. Synthesis of magnesium-modified ceramsite from iron tailings as efficient adsorbent for phosphorus removal. Separation and Purification Technology 326, 124817.

Li, X., Zhao, X., Zhou, X., Yang, B., 2021. Phosphate recovery from aqueous solution via struvite crystallization based on electrochemical-decomposition of nature magnesite. Journal of Cleaner Production 292, 126039.

Lin, J., Zhan, Y., Wang, H., Chu, M., Wang, C., He, Y., Wang, X., 2017. Effect of calcium ion on phosphate adsorption onto hydrous zirconium oxide. Chemical Engineering Journal 309, 118–129.

Lin, J.-Y., Li, D., Kim, M., Lee, I., Kim, H., Huang, C.-P., 2021. Process optimization for the synthesis of ceramsites in terms of mechanical strength and phosphate adsorption capacity. Chemosphere 278, 130239.

Liu, F., Liang, X., He, S., Li, F., Jin, Y., Zhao, Z., Zhu, L., 2021a. Performance of a new low-cost Zn/Fe-layered double hydroxide-modified ceramsite for the removal of P from agricultural runoff. Ecological Engineering 159, 106117.

Liu, M., Wang, C., Guo, J., Zhang, L., 2021b. Removal of phosphate from wastewater by lanthanum modified bio-ceramisite. Journal of Environmental Chemical Engineering 9 (5), 106123.

Liu, S., Yang, C., Liu, W., Yi, L., Qin, W., 2020. A novel approach to preparing ultra-lightweight ceramsite with a large amount of fly ash. Frontiers of environmental science & engineering 14, 1–11.

Liu, Y., Hu, X., Lei, Y., Li, F., You, S., 2021c. Carbon nanotubes functionalized with calcium carbonate for flow-through sequential electrochemical phosphate recovery. ACS ES&T Water 2 (1), 206–215.

Luo, H., Wan, Y., Cai, Y., Dang, Z., Yin, H., 2022. Enhanced phosphate adsorption by mg-stirred leaf biochar in a complex water matrix via active MgO facet exposure. ACS ES&T Engineering 2 (12), 2254–2265.

Ma, J., Qi, J., Yao, C., Cui, B., Zhang, T., Li, D., 2012. A novel bentonite-based adsorbent for anionic pollutant removal from water. Chemical Engineering Journal 200, 97–103.

Ma, Y., Zhu, J., Yu, J., Fu, Y., Gong, C., Huang, X., 2022. Adsorption Characteristics of Phosphate Based on Al-Doped Waste Ceramsite: Batch and Column Experiments. International Journal of Environmental Research and Public Health 20 (1), 671.

Mitrogiannis, D., Psychoyou, M., Baziotis, I., Inglezakis, V.J., Koukouzas, N., Tsoukalas, N., Palles, D., Kamitsos, E., Oikonomou, G., Markou, G., 2017. Removal of phosphate from aqueous solutions by adsorption onto Ca (OH) 2 treated natural clinoptilolite. Chemical Engineering Journal 320, 510–522.

Nematian, M., Keske, C., Ng'ombe, J.N., 2021. A techno-economic analysis of biochar production and the bioeconomy for orchard biomass. Waste Management 135, 467–477.

Nguyen, M.D., Thomas, M., Surapaneni, A., Moon, E.M., Milne, N.A.J.E.T. and Innovation 2022. Beneficial reuse of water treatment sludge in the context of circular economy. 28, 102651.

Pap, S., Kirk, C., Bremner, B., Sekulic, M.T., Shearer, L., Gibb, S.W., Taggart, M.A., 2020. Low-cost chitosan-calcite adsorbent development for potential phosphate removal and recovery from wastewater effluent. Water research 173, 115573.

Qiu, G., Zhao, Y., Wang, H., Tan, X., Chen, F., Hu, X., 2019. Biochar synthesized via pyrolysis of Broussonetia papyrifera leaves: mechanisms and potential applications for phosphate removal. Environmental Science and Pollution Research 26, 6565–6575.

Shan, S., Wang, W., Liu, D., Zhao, Z., Shi, W., Cui, F., 2020. Remarkable phosphate removal and recovery from wastewater by magnetically recyclable La2O2CO3/γ-Fe2O3 nanocomposites. Journal of Hazardous Materials 397, 122597.

Shi, C., Zhao, B., Guo, X., Zeng, R., Hao, L., Wang, X., Hao, X.J.S.C. and Pharmacy 2024. Synergistic recovery of aluminum phosphorus from incinerated sewage sludge ash via acid and alkaline treatment. 41, 101707.

USEPA 2004 SW-846 Chapter Seven: Characteristics Introduction and Regulatory Definitions (revision 4).

Wan, K., Huang, L., Yan, J., Ma, B., Huang, X., Luo, Z., Zhang, H., Xiao, T., 2021. Removal of fluoride from industrial wastewater by using different adsorbents: A review. Science of the Total Environment 773, 145535.

Wang, B., Hu, X., Li, L., Wang, H., Huang, H., Wang, R., Zhou, D., Yuan, J., Chen, L., 2023a. Application and functionalization of toxic waste sludge-derived biochar for efficient phosphate separation from aqueous media: toxicity diminution, robust adsorption, and inner mechanism. Chemical Engineering Journal, 143745.

Wang, B., Zhang, H., Hu, X., Chen, R., Guo, W., Wang, H., Wang, C., Yuan, J., Chen, L., Xia, S., 2023b. Efficient phosphate elimination from aqueous media by La/Fe bimetallic modified bentonite: Adsorption behavior and inner mechanism. Chemosphere 312, 137149.

Wang, C., Huang, C., Xu, H., Yuan, N., Liu, X., Bai, L., He, X., Liu, R., 2022. Ceramsite production using water treatment residue as main ingredient: The key affecting factors identification. Journal of Environmental Management 308, 114611.

Wang, H., Xu, J., Liu, Y., Sheng, L., 2021. Preparation of ceramsite from municipal sludge and its application in water treatment: A review. Journal of Environmental Management 287, 112374.

Wang, J., Liu, H., Chen, C., Zhang, S., Guo, F., Li, Y.J.E.m. and assessment 2019. The resilience research of the plant and soil optimization design base on the habitat-site design in semiarid green space. 191, 1-16.

Wang, S., Kong, L., Long, J., Su, M., Diao, Z., Chang, X., Chen, D., Song, G., Shih, K., 2018. Adsorption of phosphorus by calcium-flour biochar: Isotherm, kinetic and transformation studies. Chemosphere 195, 666–672.

Water Science and Technology Directorate 2011 Water quality status and trends of nutrients in major drainage areas of Canada: Technical Summary, Environment Canada.

Wu, B., Wan, J., Zhang, Y., Pan, B., Lo, I.M., 2019. Selective phosphate removal from water and wastewater using sorption: process fundamentals and removal mechanisms. Environmental Science & Technology 54 (1), 50–66.

Wu, L., Liu, C., Hu, Y., Tan, B., He, Y., Li, N., 2020a. Dephosphorization using ceramsites modified by coprecipitation with FeSo4 and KMnO4 and high-temperature combustion. Journal of Water Process Engineering 34, 101162.

Wu, L., Zhang, S., Wang, J., Ding, X., 2020b. Phosphorus retention using iron (II/III) modified biochar in saline-alkaline soils: Adsorption, column and field tests. Environmental Pollution 261, 114223.

Zeng, J., Chen, D., Zhu, J., Long, C., Qing, T., Feng, B., Zhang, P., 2023. Phosphate recovery using activated sludge cyanophycin: Adsorption mechanism and utilization as nitrogen-phosphorus fertilizer. Chemical Engineering Journal 476, 146607.

Zhang, X., Wang, X., Chen, Z., 2017. A novel nanocomposite as an efficient adsorbent for the rapid adsorption of Ni (II) from aqueous solution. Materials 10 (10), 1124.

Zhu, Z., Qin, L., Liu, Y., Zhang, Q., Cheng, P., Liang, W., 2024. Fabrication and mechanism of La/Al bimetallic organic frameworks for phosphate removal. Chemical Engineering Journal 479, 147081.

Ziajahromi, S., Lu, H.-C., Drapper, D., Hornbuckle, A., Leusch, F.D., 2023. Microplastics and tire wear particles in urban stormwater: abundance, characteristics, and potential mitigation strategies. Environmental Science & Technology 57 (34), 12829–12837.